Mechanisms of Development 155 (2019) 34–47

Contents lists available at ScienceDirect

Mechanisms of Development

journal homepage: www.elsevier.com/locate/mod

MiR-203a is differentially expressed during branching morphogenesis and EMT in breast progenitor cells and is a repressor of peroxidasin

Eirikur Briem[a], Zuzana Budkova[a], Anna Karen Sigurdardottir[a], Bylgja Hilmarsdottir[a,d], Jennifer Kricker[a], Winston Timp[e], Magnus Karl Magnusson[b,c], Gunnhildur Asta Traustadottir[a], Thorarinn Gudjonsson[a,b,*]

[a] Stem Cell Research Unit, Biomedical Center, Department of Anatomy, Faculty of Medicine, School of Health Sciences, University of Iceland, Iceland
[b] Department of Laboratory Hematology, Landspitali - University Hospital, Iceland
[c] Department of Pharmacology and Toxicology, Faculty of Medicine, School of Health Sciences, University of Iceland, Iceland
[d] Department of Tumor Biology, The Norwegian Radium Hospital, Oslo, Norway
[e] Department of Biomedical Engineering, Johns Hopkins University, USA

A B S T R A C T

MicroRNAs regulate developmental events such as branching morphogenesis, epithelial to mesenchymal transition (EMT) and its reverse process mesenchymal to epithelial transition (MET). In this study, we performed small RNA sequencing of a breast epithelial progenitor cell line (D492), and its mesenchymal derivative (D492M) cultured in three-dimensional microenvironment. Among the most downregulated miRNAs in D492M was miR-203a, a miRNA that plays an important role in epithelial differentiation. Increased expression of miR-203a was seen in D492, concomitant with increased complexity of branching. When miR-203a was overexpressed in D492M, a partial reversion towards epithelial phenotype was seen. Gene expression analysis of D492M and D492M$^{miR\text{-}203a}$ revealed peroxidasin, a collagen IV cross-linker, as the most significantly downregulated gene in D492M$^{miR\text{-}203a}$. Collectively, we demonstrate that miR-203a expression temporally correlates with branching morphogenesis and is suppressed in D492M. Overexpression of miR-203a in D492M induces a partial MET and reduces the expression of peroxidasin. Furthermore, we demonstrate that miR-203a is a novel repressor of peroxidasin. MiR-203-peroxidasin axis may be an important regulator in branching morphogenesis, EMT/MET and basement membrane remodeling.

Summary statement

MiR-203a is highly upregulated during branching morphogenesis of D492 breast epithelial progenitor cells and is downregulated in its isogenic mesenchymal cell line D492M. Furthermore, miR-203a is a novel suppressor of peroxidasin (PXDN), a collagen IV crosslinking agent. MiR-203a may be an important regulator of branching morphogenesis and basement remodeling in the human breast gland, possibly through its target PXDN.

1. Introduction

Developmental events underlying breast epithelial morphogenesis are closely related to pathways important to cancer progression, *i.e.* epithelial to mesenchymal transition (EMT) and mesenchymal to epithelial transition (MET). Evidence shows that the two distinct epithelial cell lineages that make up branching morphogenesis in the breast, luminal- and myoepithelial cells, originate from common breast epithelial stem cells (Pechoux et al., 1999; Gudjonsson et al., 2002; Villadsen et al., 2007; Petersen and Polyak, 2010). These stem cells are responsible for continuous tissue remodeling throughout the reproductive period, as well as the extensive epithelial expansion and branching morphogenesis seen during pregnancy and lactation. Although, potential stem or progenitor cells have been identified in the human female breast gland there is still limited knowledge about the lineage development in the human breast. In that respect much can be learned from linage tracing studies in the mouse mammary gland. Recent studies have demonstrated that embryonic mammary gland contains homogenous basal progenitor cells that become restricted in the postnatal mammary gland (Lloyd-Lewis et al., 2018). Lilja et al. demonstrated that embryonic multipotent mammary cells become lineage-restricted early in development and that gain of function dictates luminal cell fate specification to both embryonic and basally committed mammary cells (Lilja et al., 2018). In a recent article Pal et al. demonstrated by single cell profiling of four developmental stages in the post-natal gland that the epithelium undergoes large changes in gene expression (Pal et al., 2017). In this paper they show that homogeneous basal-like expression pattern in pre-puberty was distinct to lineage-restricted programs in

* Corresponding author at: Stem Cell Research Unit, Department of Medical Faculty, Biomedical Center, University of Iceland, Vatnsmyrarvegi 16, 101 Reykjavík, Iceland.
E-mail address: tgudjons@hi.is (T. Gudjonsson).

https://doi.org/10.1016/j.mod.2018.11.002
Received 29 March 2018; Received in revised form 1 November 2018; Accepted 23 November 2018
Available online 01 December 2018

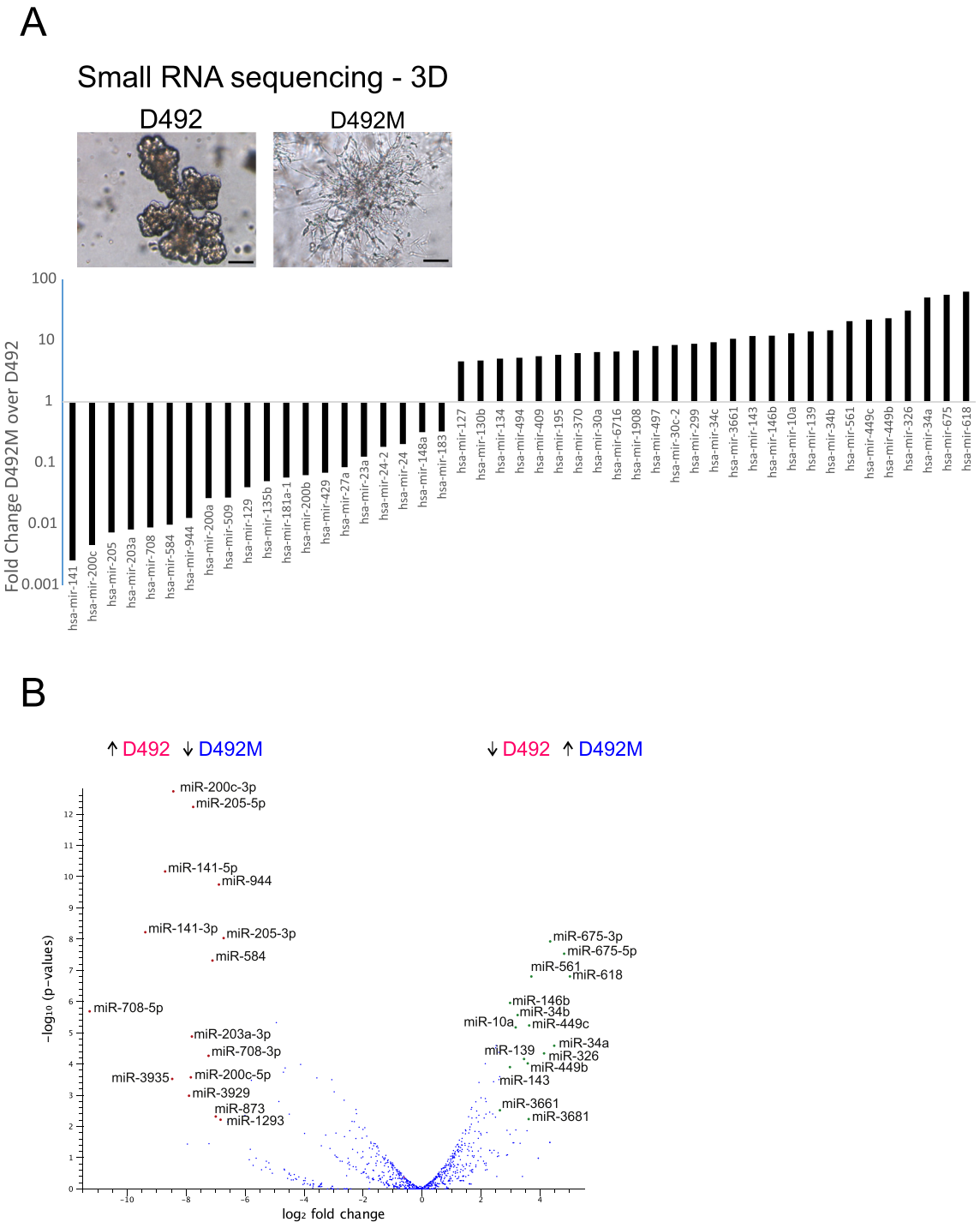

Fig. 1. Profiling miRNAs in the isogenic breast epithelial progenitor cell line D492 and its mesenchymal derivative D492M.
A) Differentially expressed miRNAs between D492M and D492 in 3D culture based on small RNA sequencing. Forty-seven miRNAs are differentially expressed between the mesenchymal (D492M) and epithelial (D492) state at day 14 in 3D culture. Twenty miRNAs are downregulated in D492M and among them are miRNAs that are important for epithelial integrity, such as the miR-200 family and miR-203a. Scale bar = 100 μm.
B) Volcano plot showing differential expressed miRNAs in D492M and D492, depicting statistical significance and high fold change in expression of epithelial associated miRNAs. Volcano plot constructed from small RNA sequencing data using fold change of expression values and p-values, enabling the visualization of the relationship between fold change and statistical significance. More extreme values on the x-axis show increased differential expression and higher values on the y-axis show increased statistical significance. The miR-200c-141 locus along with miR-205, miR-944, miR-584, miR-708 and miR-203a show the most fold change and statistical significance of the miRNAs downregulated in D492M.

puberty. Cellular linage tracing in humans is for obvious reasons not possible. However, transplantation of human breast epithelial cells into cleared mouse mammary fat pad (Lawson et al., 2015; Wronski et al., 2015) and 3D culture (Vidi et al., 2013) have to some extend unraveled the stem cell biology in the human breast gland. D492 is a breast epithelial stem cell line that generates branching *in vivo*-like structures in 3D-rBM (Gudjonsson et al., 2002; Villadsen et al., 2007; Sigurdsson et al., 2011). We have previously shown that when D492 is co-cultured

under 3D conditions, breast endothelial cells markedly stimulate their branching ability, but can also induce an irreversible EMT in the epithelial cells (Sigurdsson et al., 2011). This condition gave rise to the D492M cell line (Sigurdsson et al., 2011). In EMT, different pathways ultimately control transcriptional regulatory factors such as SNAI1, SNAI2, TWIST, ZEB1 and ZEB2 leading to increased expression of mesenchymal and decreased expression of epithelial markers (Moustakas and Heldin, 2007). Downregulation of the epithelial cell-cell adhesion proteins, such as E-cadherin, is one of the hallmarks of EMT (Peinado et al., 2007). In addition, expression of epithelial specific keratins is often greatly reduced, while expression of mesenchymal markers, such as N-cadherin, vimentin, alpha smooth muscle actin and fibronectin are increased in EMT (Moustakas and Heldin, 2007). Enhanced migration, invasion and resistance to apoptosis are also characteristic for cells that have undergone EMT (Hanahan and Weinberg, 2011). The tightly regulated process of cell conversion seen in EMT is also a critical event seen in many cancer types, including breast cancer (Petersen et al., 2001; Mani et al., 2008; Sarrio et al., 2008) and EMT is typically associated with increased aggressiveness and metastatic behavior (Hanahan and Weinberg, 2011).

Interestingly, the mesenchymal transition from D492 to D492M is accompanied by drastic changes in microRNA (miRNA) expression (Hilmarsdottir et al., 2015). MiRNAs have been described as regulators of protein expression through their ability to bind and silence mRNAs, where silencing of certain transcription factors, which are important for gene regulation, may cause marked changes in cell phenotype and fate (Hilmarsdottir et al., 2014). In recent years, miRNAs have been shown to be either tumor promoting or tumor suppressing depending on context and cancer type. For example, the miR-200 family has been linked to both stem cell regulation and cancer progression (Shimono et al., 2009). This family of miRNAs is strongly downregulated in tumors with high metastatic potential (Olson et al., 2009) and miR-200c, a member of this family, is downregulated in human breast cancer stem cells and normal mammary stem cells (Shimono et al., 2009). We have recently shown that the miRNA-200c-141 cluster is predominantly expressed in luminal breast epithelial cells, and that miRNA-200c-141 is highly expressed in D492, but not in D492M. Interestingly, overexpression of miR-200c-141 in D492M restored the luminal epithelial phenotype (Hilmarsdottir et al., 2015).

In this study, we compared the miRNA expression profile of D492 and D492M, when cultured in 3D reconstituted basement membrane matrix (3D-rBM). Small RNA sequencing revealed a striking difference in expression patterns between the two cell lines, with a number of known epithelial miRNAs, including miR-203a, downregulated in D492M. We demonstrated that miR-203a expression increases during branching morphogenesis *in vitro* similar to its expression pattern in mouse mammary gland *in vivo* (Avril-Sassen et al., 2009). Furthermore, overexpression of miR-203a in D492M induced partial phenotypic changes towards MET, reduced cell proliferation, migration, invasion, and increased sensitivity to chemically induced apoptosis. Finally, we identified miR-203a as a novel repressor of peroxidasin (PXDN), an extracellular matrix protein with peroxidase activity and a collagen IV crosslinking agent.

2. Results

2.1. Comparison of miRNA expression in the breast epithelial progenitor cell line D492 and its mesenchymal derivative D492M

D492 and D492M are isogenic cell lines with epithelial and mesenchymal phenotypes, respectively. We have previously shown a profound difference in miRNA expression between these cell lines when cultured in monolayer (Hilmarsdottir et al., 2015). Here, we conducted an expression analysis in 3D culture. Due to its stem cell properties, D492 can generate branching structures in 3D-rBM culture reminiscent of terminal duct lobular units (TDLUs) in the breast. In contrast, D492M form disorganized mesenchymal-like structures with spindle shape protrusions of cells (Fig. 1A, top). To investigate the miRNA expression patterns between D492 and D492M in 3D-rBM we performed small RNA sequencing (Fig. 1A). This revealed 47 differentially expressed miRNAs (> 1.5-fold change, $p < 0.05$ and FDR < 0.1) between D492 from (days 7, 14 and 21) and D492M at day 14 in 3D culture, where 20 of these miRNAs were downregulated in D492M. Among the most profound changes was downregulation of miR-200c, miR-141, miR-205 and miR-203a in D492M (Fig. 1A), all of which have been previously associated with epithelial integrity and repression of EMT (Gregory et al., 2008; Wellner et al., 2009; Feng et al., 2014). These miRNAs were all downregulated with high statistical significance in D492M as shown in the volcano plot (Fig. 1B). The upregulated miRNAs in D492M do not show as clear involvement in EMT as the downregulated ones.

2.2. Downregulation of miR-203a in D492M is not due to methylation of its CpG islands in the promoter area

Methylation of CpG islands in promoter areas is a common event during gene silencing. To further explore what causes downregulation of miRNAs in D492M, we explored the promoter DNA methylation status of differentially expressed miRNAs. We used the HumanMethylation450K BeadChip and looked at CpGs within 5 kb region of the promoter area of differentially expressed miRNAs. Two miRNAs did not have probes within the 5 kb region of the gene but of the 45 which did, 8 miRNAs showed differential DNA methylation between D492 and D492M (Table S2). Our data shows that promoter areas upstream of miR-200c-141 and miR-205 were methylated in D492M, but not in D492 (Fig. 2A). In contrast, the promoter area of miR-203a was not differentially methylated between D492 and D492M (Fig. 2A). Bisulfite sequencing of the promoter area of miR-200c-141, miR-205 and miR-203a confirmed that the promoter of miR-203a was unmethylated in D492M, unlike the promoters of miR-200c-141 and miR-205 (Fig. 2B). This is in contrast to previously published results in human mammary epithelial cells (HMLE) undergoing EMT (Taube et al., 2013) and some metastatic breast cancer cell lines (Zhang et al., 2011), where the promoter of miR-203a becomes methylated. Our data shows that a profound downregulation of miR-203a could be mediated through other mechanisms than DNA methylation, such as histone modifications. Indeed, miR-203a expression has been shown to be suppressed by EZH2 in prostate cancer (Cao et al., 2011). In summary, the repression of miR-203a, in endothelial induced EMT of D492 is not due to promoter methylation.

2.3. MiR-203a shows temporal changes in expression during branching morphogenesis in 3D culture and is associated with luminal breast epithelial cells

The breast gland is a dynamic organ during the reproduction period. In each menstrual cycle the breast epithelium undergoes changes associated with branching morphogenesis and if pregnancy occurs, the branching epithelium expands resulting in maximal differentiation during lactation. The glandular epithelium is then subject to apoptosis after breastfeeding during the involution phase (Javed and Lteif, 2013). Using D492 breast progenitor cells that are capable of generating branching epithelial morphogenesis in 3D-rBM, it is possible to analyze temporal changes during the branching process. To investigate if changes in miRNA expression occur during formation of TDLU–like structures in 3D-rBM, we isolated RNA from 3D-rBM cultures at days 7, 14 and 21, and performed small RNA sequencing.

Fifty-five miRNAs were differentially expressed between individual time points (> 2-fold change, FDR corrected p-value < 0.05), thereof 40 miRNAs were downregulated and 15 miRNAs were upregulated during branching (Fig. 3A). In particular, among the upregulated miRNAs were miR-141 and miR-203, which were also some of the most downregulated miRNAs in D492M (Fig. 1A). Thus, small RNA

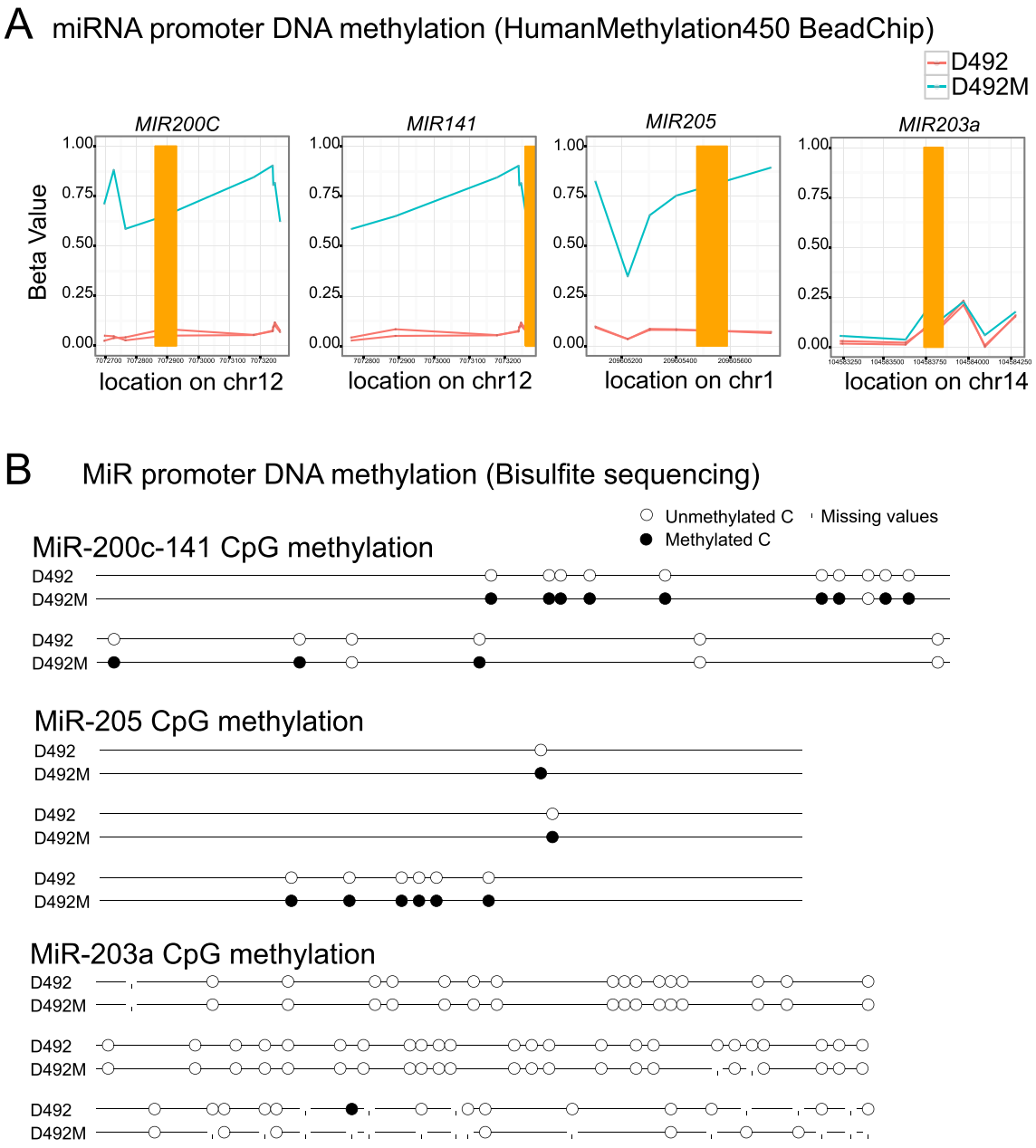

Fig. 2. miRNA promoter methylation of D492 and D492M

A) Differential DNA methylation of D492 (red) and D492M (blue). CpG methylation in the promoter area of differentially expressed miRNAs was investigated using the HumanMethylation450 BeadChip. The yellow bar represents the pre-miRNA and differential methylation is determined by a beta value > 0.2. MiR-200c, miR-141 and miR-205 are differentially methylated with more methylation in D492M, while methylation of miRNA-203a is unchanged. The expression of miR-200c-141 and miR-205 is repressed through DNA methylation, while expression of miRNA-203a is not.

B) Bisulfite sequencing of miRNA promoters in D492 and D492M. The promoters of miR-200c-141, miR-205 and miR-203a are un-methylated in D492. In D492M, the promoter of miR-203a remains un-methylated, while the promoters of miR-200c-141 and miR-205 are methylated.

sequencing, and subsequent verification with RT-qPCR, demonstrates that expression of miR-203a and miR-141 increased between time points and peaked at the late branching stage (day 21) (Fig. 3A–B). In contrast, expression of miR-205 and miR-200c was constant throughout the branching process (Fig. 3B). This indicates that miR-203a and miR-141 may play a role in differentiation of the epithelial cells during branching morphogenesis. The human breast epithelium is composed of two epithelial lineages, the luminal epithelial and the myoepithelial cells. In order to investigate whether miR-203a expression was lineage specific with either luminal- or myoepithelial cells, we sorted primary breast epithelial cells with EpCAM positive magnetic beads, as EpCAM is a luminal associated adhesion molecule that is also highly useful for antibody-based enrichment of luminal epithelial cells. We measured miR-203a expression in EpCAM high and EpCAM low cells, and demonstrated that, miR-203a expression was predominately associated with the EpCAM high luminal epithelial cells (Fig. 3C, left). There was some expression in the EpCAM low/negative myoepithelial cells, but no or little expression in endothelial cells and fibroblast (Fig. 3C, left). Due to the bipotential properties of D492 cells, they are able to generate luminal- and myoepithelial cells and differentiation of D492 branching colonies, into the two epithelial lineages, is clearly demonstrated with immunostaining against luminal- and myoepithelial markers (Gudjonsson et al., 2002). Based on EpCAM sorting of D492 cells into EpCAM high and EpCAM low fractions, we further confirmed that miR-

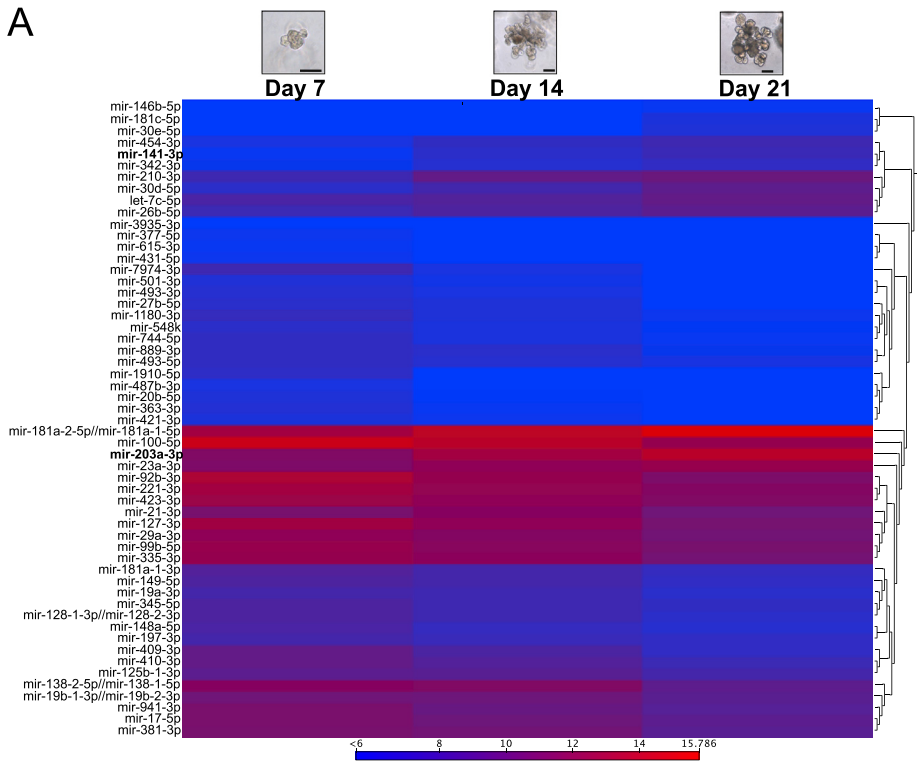

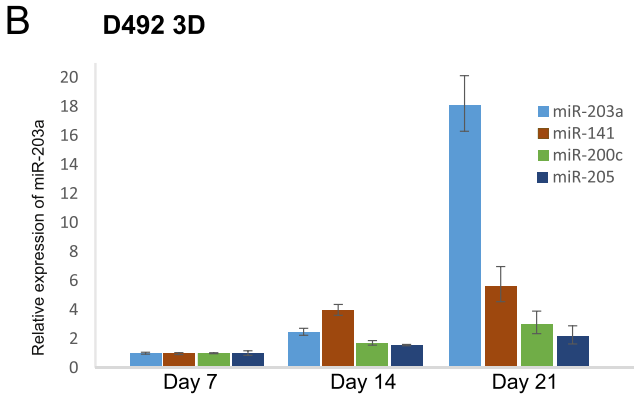

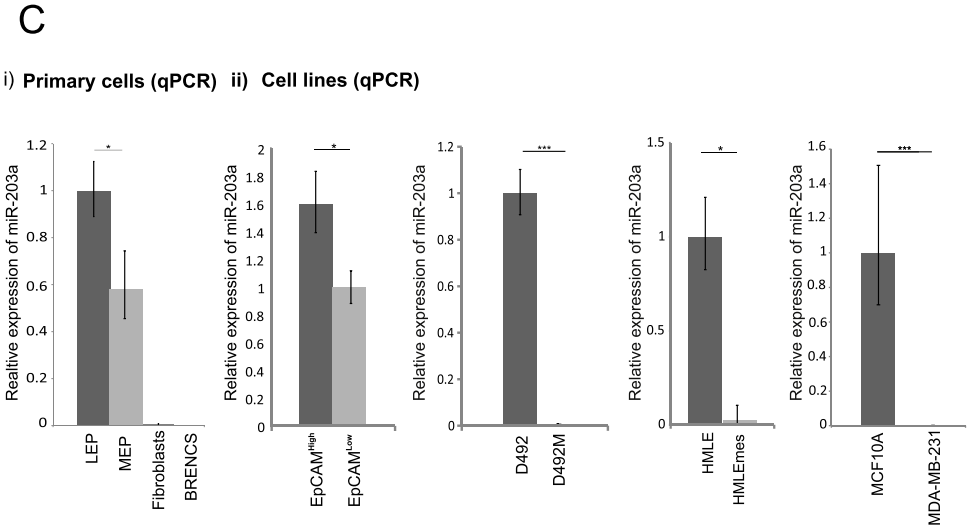

Fig. 3. MiR-203a is differentially expressed during branching morphogenesis in 3D culture.

A) Heatmap showing differentially expressed miRNAs in D492 at different time points during branching morphogenesis. Small RNA-sequencing of D492 at three different time points during branching morphogenesis at day 7, 14 and 21. miR-203a expression increases during branching of D492. Heatmap shows miRNAs with > 2-fold change in expression an FDR corrected p-values < 0.1. Scale bar = 100 μm.

B) Expression of epithelial miRNAs in D492 at different time points during branching. RT-qPCR showing that the expression of miR-203a and miR-141 significantly increases between time points during branching morphogenesis. Interestingly, expression of miR-203a increases markedly in late branching at day 21.

C) i) Expression of miR-203a in breast primary cells and D492 EpCAM sorted cells. In primary cells, miR-203a is expressed in the epithelial cells and is predominantly associated with the luminal cells but is absent in fibroblasts and endothelial cells. In D492 cells, miR-203a expression is predominantly associated with the EpCAM High cells.

ii) MiR-203a expression in breast cell lines. MiR-203a is expressed in breast cell lines with an epithelial phenotype but not with a mesenchymal phenotype. Expression of miR-203a in mesenchymal derivatives of D492 and HMLE, *i.e.* D492M and HMLEmes, is down-regulated with little or no expression in the mesenchymal state. The normal like breast cell line MCF10A has high expression of miR-203a, while the triple negative mesenchymal breast cancer cell line MDA-MB-231 has no expression of miR-203a. Results are displayed as average of three independent experiments (mean ± sd, n = 3).

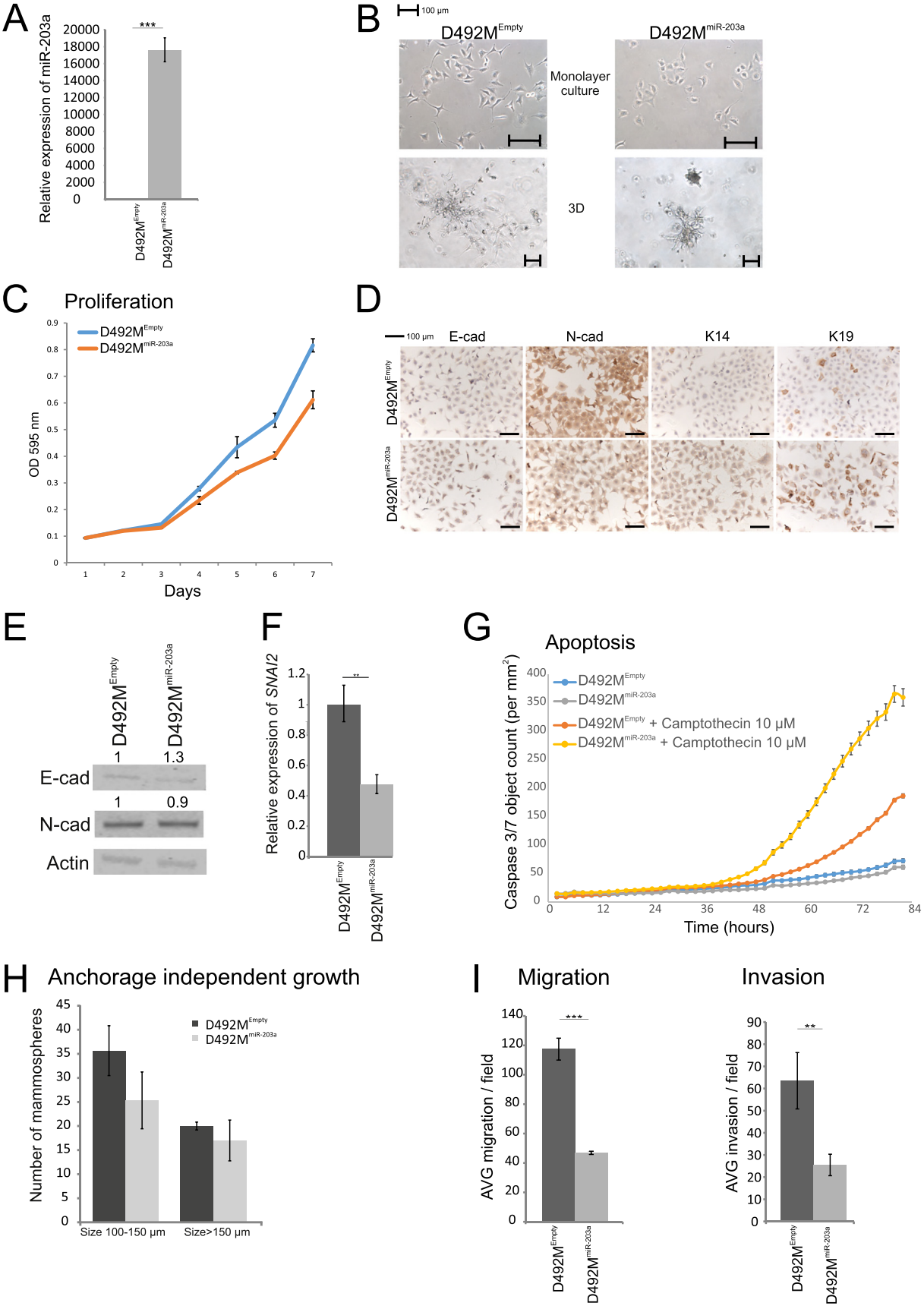

(caption on next page)

Fig. 4. Overexpression of miR-203a in D492M.
A)Overexpression of miR-203a in D492M. RT-qPCR showing 17,500-fold expression of miR-203a in D492M$^{miR\text{-}203a}$ compared to control.
B) MiR-203a increases adherence of D492M cells. Phase contrast images of monolayer cultures show that miR-203a overexpression in D492M causes cells to adhere more to each other compared to D492M^{Empty} control. Phase contrast images from 3D culture show that D492M$^{miR\text{-}203a}$ form more compact colonies, with some colonies showing protrusion of mesenchymal cells compared to control. Scale bar = 100 μm.
C) MiR-203a reduces proliferation of D492M. Reduced proliferation of D492M shown by staining with crystal violet from day 1–7 in monolayer culture. Results are shown as average of 4 replicates (mean ± SD)
D) DAB staining of monolayer cultures from D492M$^{miR\text{-}203a}$. D492M$^{miR\text{-}203a}$ cells display reduced expression of N-Cadherin but show little change in expression of E-Cadherin. Scale bar = 100 μm.
E) Western blot of E- and N-Cadherin in D492M$^{miR\text{-}203a}$. There is slightly less protein expression of N-Cadherin (10% reduction) but little change in expression of E-Cadherin in D492M$^{miR\text{-}203a}$ indicating reduced mesenchymal characteristics in D492M$^{miR\text{-}203a}$.
F) Expression of SNAI2 is reduced in D492M$^{miR\text{-}203a}$. MiR-203a, which has a known binding site in the 3′-UTR of SNAI2, significantly reduces expression of SNAI2 as determined by qPCR.
G) D492M$^{miR\text{-}203a}$ cells are more sensitive to chemically induced apoptosis. In D492M cells, miR-203a increases sensitivity to apoptosis induced by Camptothecin. Data is analyzed on IncuCyte Zoom and data is displayed as Caspase 3/7 object count/mm^2 (mean ± SEM).
H) Anchorage independent growth is reduced upon miR-203a overexpression. miR-203a reduces stem cell like properties in D492M. D492M$^{miR\text{-}203a}$ has reduced ability to generate mammospheres in low attachment assay compared to D492M^{Empty}.
I) MiR-203a reduces the ability of D492M cells to migrate and invade. D492M$^{miR\text{-}203a}$ has less ability to migrate through trans-well filter than D492M^{Empty} and D492M$^{miR\text{-}203a}$ has reduced capability to invade through Matrigel coated transwell filter. Data is shown as average number of cells per field (mean ± SEM).

203a was more associated with the luminal epithelial population in D492 (Fig. 3C, right). Differential expression of miR-203a between D492 and D492M was confirmed by RT-qPCR (Fig. 3C, right). To determine whether this was in concurrence with other breast cell lines with epithelial and mesenchymal phenotypes, we examined the expression levels of miR-203a in HMLE, its mesenchymal derivative HMLEmes (Fig. 3C, right), the normal cell-derived MCF10A, and the mesenchymal cancer cell line, MDA-MB-231 (Fig. 3C, right). Expression of miR-203a was restricted to all three cell lines with an epithelial phenotype.

2.4. MiR-203a expression reduces the mesenchymal traits of D492M cells

To analyze if the presence of miR-203a affects the phenotype of D492M, we overexpressed miR-203a in D492M (D492M$^{miR\text{-}203a}$), using a lentiviral based transfection system. D492M$^{miR\text{-}203a}$ expressed miR-203a 17,500-fold higher than control (D492M^{Empty}) (Fig. 4A). Interestingly, phase contrast images of monolayer cultures show that miR-203a overexpression in D492M causes increased adherence between cells (Fig. 4B). Furthermore, when D492M is cultivated in 3D-rBM, it forms spindle shaped mesenchymal-like colonies in contrast to D492M$^{miR\text{-}203a}$ that forms more compact colonies although the colonies still show cellular protrusions, typical of mesenchymal cells (Fig. 4B). When the cells were cultured in monolayer, overexpression of miR-203a in D492M reduces the proliferation rate of the cells (Fig. 4C). Furthermore, there was visible reduction in expression of the mesenchymal marker N-cadherin and increased expression of E-cadherin, K14 and K19 in D492M$^{miR\text{-}203a}$, indicating a moderate reduction in mesenchymal characteristics (Fig. 4D–E). The EMT transcription factor SNAI2 is a confirmed target of miR-203a, and miR-203a is in return suppressed by SNAI2 forming a negative feedback loop (Ding et al., 2013). In concordance with SNAI2 being a target of miR-203a, there was reduced expression of SNAI2 when miR-203a was overexpressed in D492M (Fig. 4F). Since the EMT phenotype has been associated with apoptosis resistance and SNAI2 is a known inhibitor of apoptosis (Inoue et al., 2002), we asked if D492M$^{miR\text{-}203a}$ cells were less resistant to chemically induced apoptosis compared to D492M^{Empty}. Indeed, D492M$^{miR\text{-}203a}$ cells were more sensitive than D492M^{Empty} to camptothecin, a chemical inducer of apoptosis (Fig. 4G).

The ability of cells to proliferate as mammospheres under non-adherent conditions has been described as a property of early progenitor/stem cells (Dontu et al., 2003). When D492 and D492M were cultured in low attachment plates both generated mammospheres but D492M generated significantly larger and a higher number of colonies (Sigurdsson et al., 2011). Interestingly, overexpression of miR-203a in D492M negatively impacts anchorage independent growth, resulting in loss of progenitor/stem cell properties indicating that miR-203a overexpression in D492M induces cellular differentiation (Fig. 4H). As mesenchymal cells have increased motility compared to epithelial cells, we analyzed the effect of miR-203a overexpression on the ability of D492M to migrate and invade. D492M$^{miR\text{-}203a}$ cells showed reduced ability to migrate through transwell filters (Fig. 4I, left) and to invade through Matrigel coated transwell filters (Fig. 4I, right) indicating a suppression of mesenchymal characteristics. Collectively, overexpressing miR-203a in D492M induced a reduction of mesenchymal characteristics, caused reduced proliferation, migration and invasion, and increased sensitivity towards chemically induced apoptosis.

2.5. Peroxidasin (PXDN) is a novel target of miR-203a

Due to the phenotypic differences between D492 and D492M in 3D culture and the fact that miR-203a is not expressed in D492M, we decided to compare the transcriptional profiling of D492, D492M and D492M$^{miR\text{-}203a}$, with emphasis on identifying novel targets of miR-203a. Herein, we identified peroxidasin (PXDN), a collagen IV cross-linking agent in the basement membrane, as the most significantly downregulated gene in D492M$^{miR\text{-}203a}$ compared to D492M (Fig. 5A). In addition, we identified three potential binding sites for miR-203a in the 3′-UTR of PXDN, one well conserved and two less conserved (Fig. 5B). To further investigate the potential interaction between miR-203a and PXDN we treated D492M and D492M$^{miR\text{-}203a}$ with miR-203a-mimic and miR-203a-inhibitor, respectively. PXDN expression was reduced (Fig. 5C, left) and increased (Fig. 5C, right) when D492M and D492M$^{miR\text{-}203a}$ were treated with miR-203a mimic and inhibitor, respectively, corroborating that miR-203a regulates PXDN expression. Furthermore, we demonstrated that PXDN expression was directly regulated by miR-203a by carrying out a dual luciferase reporter assay showing that the relative luciferase activity was significantly lower in the PXDN 3′-UTR containing the miR-203a target sequence compared with PXDN 3′-UTR with deleted miR-203a binding sequence, when transfected with miR-203a mimic (***$p < 0.001$) (Fig. 5D). This suggested that miR-203a could directly regulate the expression of PXDN through targeting its 3′-UTR. As a positive control we demonstrated significantly lower relative luciferase activity in p63 3′-UTR containing the miR-203a target sequence compared with p63 3′-UTR with deleted miR-203a binding sequence, when transfected with miR-203a mimic (**$p < 0.01$) (Fig. S1).

In order to investigate whether the observed effect of miR-203a overexpression on D492M is due to repression of PXDN, we knocked down PXDN in D492M using siRNA (Fig. S2) and analyzed the phenotypic changes in monolayer. As with miR-203a overexpression, we see reduced proliferation and increased sensitivity to chemically

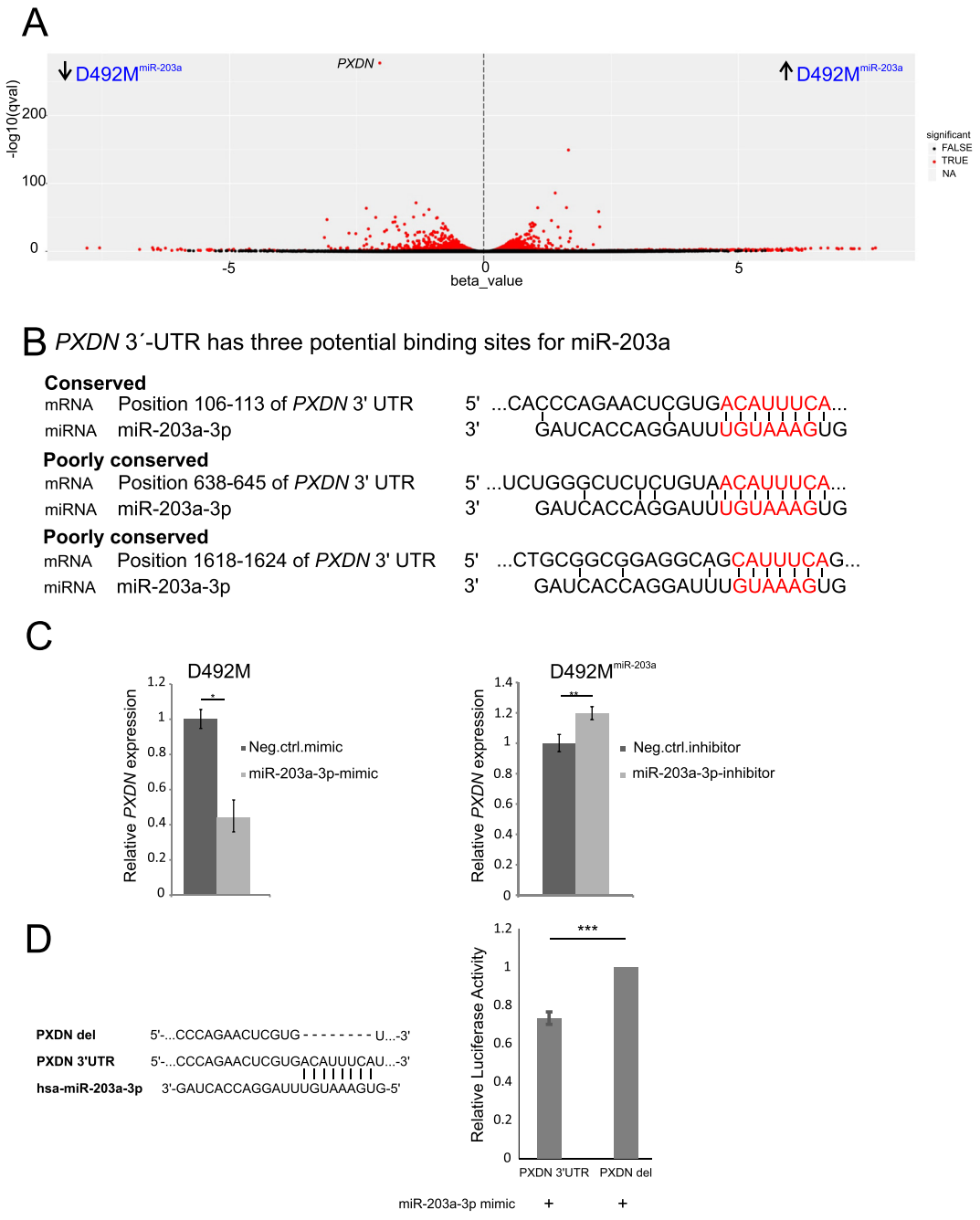

Fig. 5. Gene expression profiling of D492M overexpressing miR-203a.

A) Volcano plot showing differential expressed transcripts in D492M$^{miR\text{-}203a}$ and D492M, depicting statistical significance and high fold change in gene expression. Volcano plot was constructed from RNA sequencing data using beta and q-values from Sleuth analysis (max FDR = 0.05), enabling the visualization of the relationship between differentially expressed transcripts and statistical significance. More extreme values on the x-axis show increased differential expression and higher values on the y-axis show increased statistical significance. PXDN is the most downregulated gene when miR-203a is overexpressed in D492M.

B) PXDN 3′-UTR has three potential binding sites for miR-203a

Bioinformatics analysis reveals three potential binding sites for miR-203a in the 3′-UTR of PXDN a heme-containing peroxidase that is secreted into the extracellular matrix and is involved in extracellular matrix formation. One of the binding sites is conserved and two are poorly conserved.

C) MiR-203a regulates PXDN expression. D492M cells treated with miR-203a mimic have reduced expression of PXDN, whereas D492M$^{miR\text{-}203a}$ cells treated with miR-203a inhibitor have increased expression of PXDN. Cells were treated with miR-203a-3p mimic or inhibitor, respectively, and PXDN expression was measured by qPCR. Results are displayed as average of three independent experiments (mean ± sd, n = 3).

D) MiR-203a directly binds to its target sequence on PXDN 3′UTR. HEK293T cells transfected with miR-203a-3p mimic and pmirGLO plasmid containing the miR-203a binding site and surrounding sequence had reduced luciferase activity compared to cells transfected with the miR-203a-3p mimic and plasmid with the miR-203a binding site deleted, indicating binding of the miR-203a-3p mimic to the target sequence. Results are displayed as average of three independent experiments (mean ± SD, n = 3).

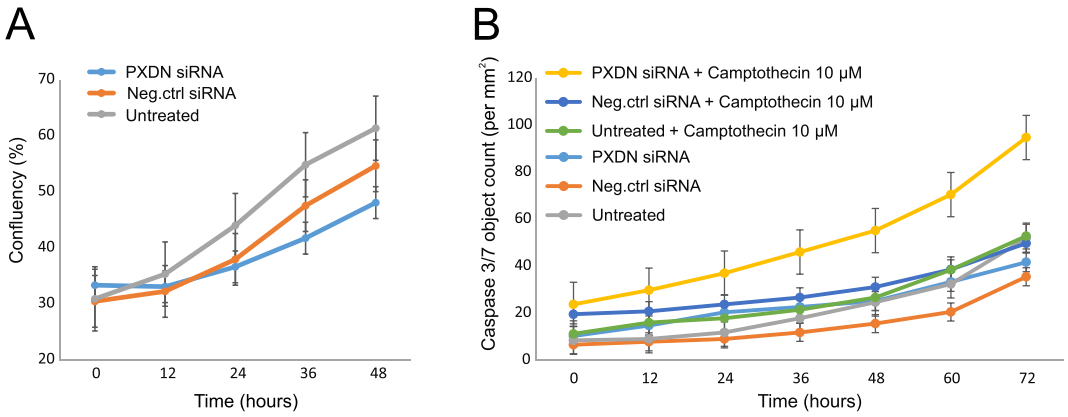

Fig. 6. PXDN repression reduces proliferation and increases sensitivity to chemically induced apoptosis.
A) PXDN silencing in D492M cells reduces proliferation. D492M cells treated with siRNA against PXDN have reduced proliferation rate compared to D492M cells treated with negative control siRNA or untreated D492M cells. Data is analyzed on IncuCyte Zoom and data is displayed as Confluency percentage (mean ± SEM). B) D492M cells with silenced PXDN are more sensitive to chemically induced apoptosis. Camptothecin induced apoptosis is increased in D492M cells with silenced PXDN, compared to cells treated with negative control siRNA and untreated D492M cells. Data is analyzed on IncuCyte Zoom and data is displayed as Caspase 3/7 object count/mm^2 (mean ± SEM).

induced apoptosis upon PXDN silencing (Fig. 6A & B), however no changes were seen in migration nor invasion (data not shown). This suggests that miR-203a mediates some of its effects, at least partly, through repression of PXDN.

Collectively, we have shown that miR-203a is a novel repressor of PXDN, a protein that plays an important role as a collagen IV cross-linking agent in the basement membrane and has been implicated in the EMT process, *i.e.* development, fibrosis and cancer.

3. Discussion

Modeling breast morphogenesis and EMT in 3D culture is an important tool to shed light on cellular and molecular mechanisms behind these developmental events and complements well *in vivo* models. Although animal models, in particular mouse models, have contributed significantly to our understanding of mammary gland morphogenesis and breast cancer, they cannot replace the necessity for using human cells due to the molecular and cellular differences in mammary gland biology between species (Dontu and Ince, 2015). Although, functionally working in similar ways during breast feeding, the mouse and human female mammary gland differ greatly. The human female breast gland is composed of ducts that end in terminal duct lobular units (TDLUs), surrounded by cellular-rich connective tissue. In contrast, the mouse mammary gland is composed of ducts that terminate in end buds, which are surrounded by adipose tissue. Thus, the histological comparison between the mouse and human mammary gland demonstrates large differences that need to be taken into account when studies are designed to explore the interactions between epithelial cells and stroma.

In this study, we have applied two isogenic breast cell lines, D492 and D492M, and 3D culture based on reconstituted basement membrane (rBM) to capture the phenotypic architecture of branching morphogenesis of breast epithelium and EMT, respectively. D492 is a breast epithelial progenitor cell line established from suprabasal epithelium of a normal breast gland (Gudjonsson et al., 2002; Villadsen et al., 2007; Sigurdsson et al., 2011). D492, was established by immortalizing cells from reduction mammoplasty using the E6 and E7 oncogenes from human papilloma virus 16. E6 and E7 target p53 and RB, respectively that without any doubt interfere with number of processes in the cells and this should be kept in mind when designing projects involving this cell line. However, D492 is non-tumorigenic, can generate both luminal and myoepithelial cells and in 3D culture generate structures reminiscent of TDLU-like structures *in vivo* and therefore remains a good tool for studying molecular mechanisms involved in these processes. D492M has a mesenchymal phenotype and is derived from D492 cells that have undergone EMT when co-cultured with breast endothelial cells (Sigurdsson et al., 2011).

In a previous work we demonstrated that overexpression of miR-200c-141 in D492M was sufficient to induce MET in D492M albeit only to luminal epithelial cells. When p63 was overexpressed in D492M containing miR-200c-141, bipotential and branching properties of D492 were restored (Hilmarsdottir et al., 2015). Recently, Wuidart et al. showed that p63 was essential for maintaining the unipotent basal fate of embryonic mouse mammary gland progenitors. Interestingly, sustained p63 expression in luminal epithelial cells reprogrammed cells towards basal cells (Wuidart et al., 2018). D492 has stem cell properties based on its ability to generate luminal and myoepithelial cells in culture and branching structures in 3D culture. It is however, possible that the immortalization using the E6 and E7 oncogenes from human papilloma virus 16 (Gudjonsson et al., 2002) and the 3D cell culture condition may contribute to the cellular plasticity of D492 and thus reflect more embryonic development of the mammary gland than postnatal development.

In this study, we analyzed differential expression of miRNAs in D492 and D492M on day 14 in 3D-rBM culture. Small RNA sequencing analysis revealed 47 differentially expressed miRNAs between D492 and D492M at day 14 in culture, of which 20 miRNAs were downregulated in D492M. Among the most profound changes, was the downregulation of the miR-200 family, miR-205 and miR-203a in D492M. We have previously shown that these miRNAs are also downregulated in D492M when cultured in monolayer (Hilmarsdottir et al., 2015) indicating a comparable expression pattern between 2D and 3D conditions. In the same study we demonstrated that when miR-141 and miR-200c, which are under regulation of the same promoter on chromosome 12 (Hilmarsdottir et al., 2014; Hilmarsdottir et al., 2015), were overexpressed in D492M, a reversal towards epithelial phenotype was induced, albeit only towards the luminal epithelial phenotype (Hilmarsdottir et al., 2015). Unlike miR-200c-141 and miR-205, which are both heavily methylated in D492M, we did not observe any methylation of CpG islands in the promoter area of miR-203a. The unmethylated pattern of the miR-203a promoter in D492M is opposite to what has been described in other breast cell lines with a mesenchymal phenotype (Zhang et al., 2011; Taube et al., 2013). This indicates that miR-203a down regulation in D492M may be through other processes, such as histone modification, or transcription factor repression.

Ectopic overexpression of miR-203a in D492M partially induced epithelial traits. The effect of increased miR-203a expression was

primarily evident in functional assays, where it caused reduced cell proliferation, migration, and invasion. Morphologic and gene expression changes were subtle and indicated only partial MET, as evidenced by reduced expression of N-cadherin, and SNAI2, an EMT transcription factor known to silence expression of miR-203a. Moes et al. demonstrated that overexpression of SNAI1 in MCF-7 breast cancer cells resulted in repression of miR-203 (Moes et al., 2012).

Branching morphogenesis of the D492 cells in 3D-rBM was used to mimic breast development and differentiation. We show that miR-203a expression coincides with increased differentiation status of the breast epithelial cells. In contrast, other epithelial associated miRNAs such as miR-205, miR-200c and miR-141 show constant or minimal fluctuation in expression throughout the branching period (21 days). In a miRNA expression study on mouse mammary gland development, Avril-Sassen et al. (2009) demonstrated that miR-203a showed temporal changes during different phases of mammary gland development. High expression was seen in early development and gestation followed by low expression in lactation and involution stages (Avril-Sassen et al., 2009). Reduced expression of miR-203a in lactation might be due to that fact that lactation requires functionally active p63 positive myoepithelial cells. MiR-203a is a repressor of p63 and therefore, downregulation of miR-203a is probably necessary for full activity of the myoepithelium.

Since D492 cells have stem cell properties, it is possible to separate cells into luminal epithelial and myoepithelial cells (Gudjonsson et al., 2002; Villadsen et al., 2007). Based on EpCAM, a luminal associated epithelial adhesion molecule, we separated D492 cells into two cell populations: EpCAM-high and EpCAM-low. EpCAM-high cells showed significantly higher expression of miR-203a than EpCAM-low cells. This was also confirmed in primary luminal epithelial- and myoepithelial cells. This result is in agreement with DeCastro et al. (DeCastro et al., 2013), where they demonstrated that miR-203a was significantly more expressed in mouse luminal epithelial progenitor cells and differentiated luminal epithelial cells compared to stem/basal cells. They also tested the expression levels of miR-203a in a number of normal and cancerous human breast epithelial cell lines: highest expression was predominantly in cell lines with a luminal epithelial phenotype.

To search for potential target genes for miR-203a we analyzed gene expression of D492M and D492M$^{miR\text{-}203a}$. The most significantly differential expressed gene between D492M and D492M$^{miR\text{-}203a}$ was PXDN. PXDN is a heme-containing peroxidase that produces hypobromous acid (HOBr) to form sulfilimine cross-links to stabilize the collagen IV network in the basement membrane and is believed to be important in normal development (Colon et al., 2017). PXDN has also been linked to EMT and disease conditions such as melanoma invasion and fibrosis (Tindall et al., 2005; Cheng et al., 2008; Peterfi et al., 2009; Liu et al., 2010; Tauber et al., 2010; Barnett et al., 2011; Khan et al., 2011; Bhave et al., 2012; Yan et al., 2014; Ero-Tolliver et al., 2015; Colon and Bhave, 2016; Jayachandran et al., 2016; Sitole and Mavri-Damelin, 2018).

Jayachandran et al. identified PXDN as consistently elevated in invasive mesenchymal-like melanoma cells and it was also found highly expressed in metastatic melanoma tumors. Gene silencing led to reduced melanoma invasion *in vitro* (Jayachandran et al., 2016). Moreover, Peterfi et al. have shown that PXDN is secreted from myofibroblasts and also from fibrotic kidney (Peterfi et al., 2009). Young et al. demonstrated that PXDN expression increases in PIK3CA mutant MCF10A cells and that the PXDN protein is mainly associated with secreted exosomes (Young et al., 2015). When knocking down PXDN in four basal like breast cancer cell lines, all cell lines showed reduced proliferation and when PXDN was knocked down in the luminal cell line MDA-MB-361, which expresses little PXDN, there was also reduced proliferation (Young et al., 2015). The reduced proliferation rate we saw in D492M$^{miR\text{-}203a}$, could be because of PXDN silencing by miR-203a, as we also see reduced proliferation when PXDN is transiently knocked down with silencing RNA. The fact that PXDN is overexpressed in the mesenchymal cell line D492M may link it to the EMT phenotype.

In summary, mammary gland development is mostly a post-natal process, where post-transcriptional regulation *via* miR-203a expression correlates with differentiation stages in the mammary epithelium. Using the D492 breast progenitor cells cultivated in 3D-rBM it is possible to capture the critical aspects of branching morphogenesis. Temporal changes in miR-203a expression during the *in vitro* branching process correlate well with *in vivo* conditions. Although miR-203a repression and overexpression are well documented in a number of studies, we observed only subtle changes towards MET when overexpressed in D492M. Furthermore, we have demonstrated a novel link between miR-203a and PXDN, which is highly expressed in D492M. Collectively, we conclude that miR-203a may be important to retain epithelial phenotype of breast epithelial cells, possibly through its target PXDN.

4. Material and methods

4.1. Cell culture

D492 and D492M cells were maintained in H14 medium as described previously (Sigurdsson et al., 2011). Primary luminal epithelial cells (EpCAM$^+$) and myoepithelial cells (EpCAM$^-$) were isolated from primary culture of breast epithelial cells derived from reduction mammoplasties by magnetic cell sorting (MACS) and maintained in CDM3 and CDM4, respectively, as previously described (Pechoux et al., 1999). Primary human breast endothelial cells (BRENCs) were isolated from breast reduction mammoplasties and cultured in endothelial growth medium (EGM) (Lonza) + 5% FBS (Invitrogen), referred to as EGM5 (Sigurdsson et al., 2006). Growth factor reduced reconstituted basement membrane (rBM, purchased as Matrigel, Corning #354230) was used for 3D cultures. 3D monocultures were carried out in 24-well culture plates (Corning). 1×10^4 D492 cells were suspended in 300 µl of rBM. Co-culture experiments were carried out with either 500, or 1×10^3 cells mixed with 1×10^5–2×10^5 BRENCs. 300 µl of mixed cells/rBM were seeded in each well of a 24-well plate and cultured on H14 (monoculture) or EGM5 (co-culture) for 14–21 days.

Branching, solid and spindle-like structures were isolated from 3D co-cultures with gentle shaking on ice in PBS - EDTA (5 mM) solution as previously described (Lee et al., 2007).

4.2. Small RNA sequencing

Total RNA was isolated from branching and spindle-like colonies from D492 and D492M, respectively using Tri-Reagent (Thermo Fisher Scientific, #AM9738). For D492 branching time points, RNA was isolated from 3D-rBM culture on days 7, 14 and 21 but for D492M RNA was isolated only on day 14. Samples were pooled in triplicates from each time point before small RNA library preparation. Small RNA libraries were prepared using the TruSeq Small RNA Library Kit from Illumina (#RS-200-0012) per manufacturer's protocol. The small RNA libraries were then sequenced using the Illumina MiSeq platform and V2 sequencing chemistry. FASTQ files were generated with MiSeq Reporter (Illumina, San Diego, US-CA). Small RNA sequence analysis was performed using the CLC Genomics Workbench (CLC Bio-Qiagen, Aarhus, Denmark) and miRBase – release 21 was used for annotation. Samples were normalized by totals and counts reported as reads per million. Reads above 29 nt and below 15 nt in length were discarded. Proportion-based statistical analysis was done using the test of Kal (Kal et al., 1999). Hierarchal clustering of features was performed using Log2 transformed expression values, Euclidean distance and single linkage. For the D492 and D492M comparison samples from day 7, 14 and 21 from D492 were compared to D492M sample from day 14.

4.3. DNA isolation and methylation bead chip array

D492 (1×10^4 cells) and D492M (2.5×10^4 cells) were grown in

3D-rBM in triplicate in a 24-well plate for 14 days and colonies extracted from 3D-rBM with gentle shaking on ice in PBS - EDTA (5 mM) solution as previously described (Lee et al., 2007). DNA was extracted using the PureLink Genomic DNA Mini Kit (Thermo Fisher Scientific, #K182002) and DNA was bisulfite converted using the EZ-96 DNA Methylation-Gold Kit (Zymo Research, #D5007) per manufacturer's protocols. The samples were hybridized to the Infinium HumanMethylation450 BeadChip array (Illumina, # WG-314-1003). Data was analyzed using the minfi Bioconductor package (Aryee et al., 2014).

4.4. Bisulfite sequencing

DNA (0.5–1 μg) was bisulfite converted using the EpiTect Bisulfite Kit (Qiagen, #59104). Target DNA sequences were amplified using nested PCR (see primers in Table S1). Methylation levels were analyzed by sequencing the bisulfite modified promoter regions on a 3130 Genetic Analyzer (Applied Biosystems). Methylation data from bisulfite sequencing was analyzed and visualized using the BiQ Analyzer v2.0 (Bock et al., 2005).

4.5. Quantitative reverse transcription PCR analysis

Total RNA was extracted with Tri-Reagent (Thermo Fisher Scientific, #AM9738) and

reverse transcription performed using random hexamers (Thermo Fisher Scientific, #N8080127) and SuperScript IV Reverse Transcriptase (Thermo Fisher Scientific, #18090050). The following primers were used for mRNA qRT-PCR analysis, SNAI2 (Hs00950344_m1) (Thermo Fisher Scientific, #4331182) and GAPDH as endogenous reference gene (Thermo Fisher Scientific, # 4326317E). Maxima Probe/ROX qPCR Master Mix (2×) (Thermo Fisher Scientific, # K0231) was used for TaqMan qRT-PCR analysis.

Quantitative RT-PCR analysis of miRNAs was performed using the universal cDNA synthesis kit II (Exiqon, #203301) and ExiLENT SYBR Green master mix (Exiqon, #203402). The following primer sets from Exiqon were used for miRNA qRT-PCR analysis, hsa-miR-203a (#205914), hsa-miR-141-3p (#204504), hsa-miR-200c-3p (#204482), hsa-miR-205-5p (#204487) and U6 snRNA (#203907) was used as endogenous reference. All qRT-PCRs were performed on the Applied Biosystems 7500 Real-Time PCR system and relative expression differences were calculated with the $2^{\Delta Ct}$ method.

4.6. Cloning of miR-203a into pCDH lentivector

The miR-203a miRNA construct was amplified from D492 genomic DNA using nested PCR with the following outer primers, miR-203a-outer-F 5′-ATCAGTCGCGGGACCTATG-3′ and miR-203a-outer-R 5′-GAATTCCACGGAGTTTCGAG-3′. From miR-203a-outer amplicon, *Eco*RI and *Not*I restriction sites were incorporated with PCR using the following inner primers, miR-203a-EcoRI-F-5′-TAAGCAGAA TTCaggcgagggcgtctaagg-3′ and miR-203a-NotI-R-5′-TGCTTAGCGGC CGCacctcccagcagcacttg-3′. Phusion High-Fidelity DNA Polymerase (NEB, # M0530S) was used for PCR and amplicons were purified using the GeneJET PCR purification kit (Thermo Fisher Scientific, #K0701). Double digestions of miR-203a-inner amplicon and pCDH vector (System Biosciences, #CD516B-2) were performed using EcoRI (NEB, #R0101) and NotI (Thermo Fisher Scientific, #ER0591). The miR-203a-inner amplicon was cloned into pCDH lentivector at insert-to-vector molar ratio 10:1 using T4 DNA ligase (Thermo Fisher Scientific, #15224041). Empty pCDH lentivector and miR-203a-pCDH lentivector were transformed into *E. coli* DH5alpha competent cells and inserts confirmed with colony PCR. Lentivectors were produced in cultures of DH5alpha and isolated using GeneJET Plasmid Miniprep kit (Thermo Fisher Scientific, #K0502). The cloned miR-203a insert sequence was then confirmed with sequencing. The pCDH lentivector has a RFP +Puro fusion containing the T2A element to enable co-expression of balanced levels of RFP and Puro genes. Viral particles were produced in HEK-293 T cells using TurboFect transfection reagent (Thermo Fisher Scientific, #R0531) and virus containing supernatant collected after 48 and 72 h, centrifuged and filtered through 0.45 μm filter. Target cells were transfected with virus titer in the presence of 8 μg/μl polybrene. Stable cell lines and control (empty-lentivector) cells were isolated with puromycin (2 μg/ml) (Thermo Fisher Scientific, # A1113803) followed by flow-sorting (Sony SH800), selecting for RFP expressing cells.

4.7. Immunochemistry

The following primary antibodies were used for DAB staining (Dako, # K3467), E-cadherin (BD, # 610182), *N*-cadherin (BD, # 610921), K14 (Abcam, #ab7800) and K19 (Abcam, #ab7754). Specimens were visualized on a Leica DMI3000 B inverted microscope.

4.8. Western blotting

Equal amounts (5 μg) of proteins in RIPA buffer were separated on NuPAGE™ 10% Bis-Tris Protein Gels (Thermo Fisher Scientific, #NP0302BOX) and transferred to a PVDF membrane (Millipore, #IPFL00010). Antibodies: SNAI2 (Cell Signaling, #9585) and Histone H3 (Cell Signaling, #4499). Secondary antibodies were mouse or rabbit IRDey (Li-Cor) used at 1:20,000 and detected using the Odyssey Infrared Imaging System (Li-Cor). Fluorescent images were converted to gray scale.

4.9. Proliferation assay

Cells were seeded in triplicates in 24-well plates and cultures stopped every 24 h. Cells were fixed in 3.7% formaldehyde in PBS for 10 min, washed once with 1 x PBS, stained with 0.1% crystal violet in 10% ethanol for 15 min, washed four times with water and dried. Density of cells was evaluated by extracting the crystal violet stain in 10% acetic acid and measuring optical density at 595 nm using a spectrometer. In addition, proliferation rate of D492M cells treated with siRNA was analyzed on IncuCyte Zoom (Essen Bioscience) per manufacturer's instructions.

4.10. Apoptosis assay

Resistance to chemically induced apoptosis with 10 μM camptothecin (Sigma-Aldrich, #C9911) was determined using IncuCyte Caspase-3/7 Reagents (Essen Bioscience, #4440) and imaging on IncuCyte Zoom (Essen Bioscience) per manufacturer's instructions.

4.11. Anchorage independence, migration and invasion assays

Anchorage independent growth was determined using 24-well ultra-low attachment plates (Corning, #3473), where triplicates of 500 cells of $D492M^{miR\text{-}203a}$ and $D492M^{Empty}$ were single cell filtered and cultured using EGM5 medium for 9 days.

For migration analysis, triplicates of 10,000 starved $D492M^{miR\text{-}203a}$ and $D492M^{Empty}$ cells were seeded in DMEM/F12, HEPES medium (Thermo Scientific, #31330038) on collagen I (Advanced BioMatrix, #5005-B) coated transwell filters with 8 μm pore size (Corning, #353097) with EGM5 medium in the lower chamber and incubated for 24 h. Filters were rinsed with 1 × PBS and cells on the apical layer wiped off with a cotton swab (Q-tip) and migrated cells fixed in 3.7% formaldehyde in PBS for 10 min, washed with 1 × PBS, stained with 0.1% crystal violet in 10% ethanol for 15 min and washed with water and then dried. Images were acquired and migrated cells counted, 3 images per filter.

Invasion assay was performed using transwell filters with 8 μm pore size (Corning, #353097) that were coated with 100 μl diluted Matrigel

(Corning, #354230) 1:10 in H14 media. D492M$^{miR-203a}$ and D492M^{Empty} (25,000 cells) were seeded in H14 media on top of Matrigel coated filters and H14 + 5% FBS added to the lower chamber and incubated for 44 h. Matrigel was then removed with a cotton swab and washed with PBS. Cells were fixed in 3.7% formaldehyde in PBS for 15 min and washed four times with water. Images were acquired and migrated cells counted, 3 images per filter.

4.12. PolyA mRNA sequencing and analysis

RNA was isolated from 3D and 2D cultures using the Exiqon miRCURY RNA Isolation Kit - Cell and Plant and quality control of RNA samples was performed using BioAnalyzer. Libraries were prepared using polyA mRNA library kit from Illumina and sequenced on a HiSeq sequencer from Illumina. Alignment of reads and annotation was performed using Kallisto (Bray et al., 2016) and differential expression analysis was done using Sleuth (Pimentel et al., 2017).

4.13. Transient transfection with miR-203a mimic

Briefly, D492M cells were separately transfected with 50 pmol of mirVANA miR-203a-3p mimic (Thermo Fisher, #4464066, Assay ID MC10152) and miRNA mimic negative control #1 (Thermo Fisher, #4464058) using RNAiMAX (Thermo Fisher, #13778075) per manufacturer's instructions for mirVana miRNA mimics.

4.14. Transient transfection with miR-203a inhibitor

Briefly, D492M$^{miR-203a}$ cells were separately transfected with 50 pmol of mirVANA miR-203a-3p inhibitor (Thermo Fisher, # 4464084, Assay ID MH10152) and mirVana miRNA Inhibitor, Negative Control #1 (Thermo Fisher, # 4464076) using RNAiMAX (Thermo Fisher, #13778075) per manufacturer's instructions for mirVana miRNA inhibitors.

4.15. Plasmid vector constructs and Luciferase activity assay

Synthetic oligonucleotides containing the hsa-miR203a-3p target sequence of human PXDN 3′-UTR (Position 106–113) or a deletion thereof (Table 1) were cloned into pmirGLO Dual-Luciferase miRNA Target Expression Vector (Promega Corporation, Madison, WI, USA). As a positive control we cloned the target sequence of p63 3′-UTR, a known hsa-miR203a-3p target, into pmirGLO, as well as a mismatched version of the p63 target site or a deletion thereof (Fig. S1). Correct sequence and orientation was verified by DNA sequencing (Eurofins Genomics, Ebersberg, Germany).

HEK293T cells were plated in a 96-well plate 3.0×10^4per well and incubated overnight. Cells were first transfected with hsa-miR203a-3p mimics (mirVana™ miRNA Mimics, Thermo Fisher Scientific, #4464070) with final concentration of 100 nM, using Lipofectamine RNAiMAX (Thermo Fisher Scienttific, #13778150) transfection reagent (according to manufacturer's instructions, with minor changes: using serum free and antibiotic-free high glucose DMEM medium instead of Opti-MEM® Medium). 24 h after transfection with miRNA mimics, cells were transfected (according to manufacturer's instructions) with 200 ng/well luciferase plasmids (pmirGLO constructs), using Lipofectamine 3000 (Thermo Fisher Scientific, #L3000015). After 24 h, plasmid-transfection cells were analyzed for luciferase activity using the Dual-Glo® Luciferase Assay System (Promega Corporation, Madison, WI, USA). Results are displayed as normalized firefly luciferase activity (background subtracted firefly luciferase activity/background subtracted renilla luciferase activity) for each construct. For each transfection, luciferase activity was averaged from four replicates, and three independent experiments were performed.

4.16. Transient transfection with siRNA

D492M cells were transfected with 10 nm final concentration of negative control siRNA (SilencerSelect siRNA #4390843, Ambion) and siRNA targeting PXDN (SilencerSelect siRNA #4427037, Ambion), using Lipofectamine RNAiMAX (Thermo Fisher Scienttific, #13778150), according to the manufacturer's protocol. Cells were incubated for 48 h and then the knockdown was confirmed by qRT-PCR using the following primers; Hs.PT.58.630748 (PrimeTime, IDT).

4.17. Statistics

All analyses comprised at least three independent experiments. Two-tailed student *t*-test was used to test significance ($p < 0.05$).

Supplementary data to this article can be found online at https://doi.org/10.1016/j.mod.2018.11.002.

Acknowledgements

We thank Erik Knutsen and Isac Lee for their contribution to this work.

Competing interests

No competing interests declared.

Funding

This work was supported by Grants from Landspitali University Hospital Science Fund, University of Iceland Research Fund, and Icelandic Science and Technology Policy - Grant of Excellence: 152144051. 'Göngum saman', a supporting group for breast cancer research in Iceland (www.gongumsaman.is). The funders had no role in study design, data collection and analysis, decision to publish, or preparation of the manuscript. Primary cells were received from reduction mammoplasty after acquiring informed consent from the donor. Approved by the Icelandic National Bioethics Committee VSN-13-057.

Data availability

NCBI GEO: https://www.ncbi.nlm.nih.gov/geo/query/acc.cgi?acc=GSE112306

The data discussed in this publication have been deposited in NCBI's

Table 1
Synthetic oligonucleotides containing the hsa-mir-203a-3p target sequence of human PXDN 3′-UTR/p63 3′-UTR or a deletion thereof.

PXDN 3′-UTR sense	/5Phos/AAACTAGCGGCCGCTAGTCCCAGAACTCGTGACATTTCATT
PXDN 3′-UTR antisense	/5Phos/CTAGAATGAAATGTCACGAGTTCTGGGACTAGCGGCCGCTAGTTT
PXDN del sense	/5Phos/AAACTAGCGGCCGCTAGTCCCAGAACTCGTGTT
PXDN del antisense	/5Phos/CTAGAACACGAGTTCTGGGACTAGCGGCCGCTAGTTT
p63 3′-UTR sense	/5Phos/AAACTAGCGGCCGCTAGTGAATGAGTCCTTGATTTCAAAT
p63 3′-UTR antisense	/5Phos/CTAGATTTGAAATCAAGGACTCATTCACTAGCGGCCGCTAGTTT
p63 del sense	/5Phos/AAACTAGCGGCCGCTAGTGAATGAGTCCTTGAT
p63 del antisense	/5Phos/CTAGATCAAGGACTCATTCACTAGCGGCCGCTAGTTT

Gene Expression Omnibus (Edgar et al., 2002) and are accessible through GEO Series accession number GSE112306.

(https://www.ncbi.nlm.nih.gov/geo/query/acc.cgi?acc=GSE112306).

References

Aryee, M.J., Jaffe, A.E., Corrada-Bravo, H., Ladd-Acosta, C., Feinberg, A.P., Hansen, K.D., Irizarry, R.A., 2014. Minfi: a flexible and comprehensive Bioconductor package for the analysis of Infinium DNA methylation microarrays. Bioinformatics 30 (10), 1363–1369.

Avril-Sassen, S., Goldstein, L.D., Stingl, J., Blenkiron, C., Le Quesne, J., Spiteri, I., Karagavriilidou, K., Watson, C.J., Tavare, S., Miska, E.A., Caldas, C., 2009. Characterisation of microRNA expression in post-natal mouse mammary gland development. BMC Genomics 10, 548.

Barnett, P., Arnold, R.S., Mezencev, R., Chung, L.W., Zayzafoon, M., Odero-Marah, V., 2011. Snail-mediated regulation of reactive oxygen species in ARCaP human prostate cancer cells. Biochem. Biophys. Res. Commun. 404 (1), 34–39.

Bhave, G., Cummings, C.F., Vanacore, R.M., Kumagai-Cresse, C., Ero-Tolliver, I.A., Rafi, M., Kang, J.S., Pedchenko, V., Fessler, L.I., Fessler, J.H., Hudson, B.G., 2012. Peroxidasin forms sulfilimine chemical bonds using hypohalous acids in tissue genesis. Nat. Chem. Biol. 8 (9), 784–790.

Bock, C., Reither, S., Mikeska, T., Paulsen, M., Walter, J., Lengauer, T., 2005. BiQ analyzer: visualization and quality control for DNA methylation data from bisulfite sequencing. Bioinformatics 21 (21), 4067–4068.

Bray, N.L., Pimentel, H., Melsted, P., Pachter, L., 2016. Near-optimal probabilistic RNA-seq quantification. Nat. Biotechnol. 34 (5), 525–527.

Cao, Q., Mani, R.S., Ateeq, B., Dhanasekaran, S.M., Asangani, I.A., Prensner, J.R., Kim, J.H., Brenner, J.C., Jing, X., Cao, X., Wang, R., Li, Y., Dahiya, A., Wang, L., Pandhi, M., Lonigro, R.J., Wu, Y.M., Tomlins, S.A., Palanisamy, N., Qin, Z., Yu, J., Maher, C.A., Varambally, S., Chinnaiyan, A.M., 2011. Coordinated regulation of polycomb group complexes through microRNAs in cancer. Cancer Cell 20 (2), 187–199.

Cheng, G., Salerno, J.C., Cao, Z., Pagano, P.J., Lambeth, J.D., 2008. Identification and characterization of VPO1, a new animal heme-containing peroxidase. Free Radic. Biol. Med. 45 (12), 1682–1694.

Colon, S., Bhave, G., 2016. Proprotein convertase processing enhances Peroxidasin activity to reinforce collagen IV. J. Biol. Chem. 291 (46), 24009–24016.

Colon, S., Page-McCaw, P., Bhave, G., 2017. Role of Hypohalous acids in basement membrane homeostasis. Antioxid. Redox Signal. 27 (12), 839–854.

DeCastro, A.J., Dunphy, K.A., Hutchinson, J., Balboni, A.L., Cherukuri, P., Jerry, D.J., DiRenzo, J., 2013. MiR203 mediates subversion of stem cell properties during mammary epithelial differentiation via repression of DeltaNP63alpha and promotes mesenchymal-to-epithelial transition. Cell Death Dis. 4, e514.

Ding, X., Park, S.I., McCauley, L.K., Wang, C.Y., 2013. Signaling between transforming growth factor beta (TGF-beta) and transcription factor SNAI2 represses expression of microRNA miR-203 to promote epithelial-mesenchymal transition and tumor metastasis. J. Biol. Chem. 288 (15), 10241–10253.

Dontu, G., Ince, T.A., 2015. Of mice and women: a comparative tissue biology perspective of breast stem cells and differentiation. J. Mammary Gland Biol. Neoplasia 20 (1–2), 51–62.

Dontu, G., Abdallah, W.M., Foley, J.M., Jackson, K.W., Clarke, M.F., Kawamura, M.J., Wicha, M.S., 2003. In vitro propagation and transcriptional profiling of human mammary stem/progenitor cells. Genes Dev. 17 (10), 1253–1270.

Edgar, R., Domrachev, M., Lash, A.E., 2002. Gene expression omnibus: NCBI gene expression and hybridization array data repository. Nucleic Acids Res. 30 (1), 207–210.

Ero-Tolliver, I.A., Hudson, B.G., Bhave, G., 2015. The ancient immunoglobulin domains of peroxidasin are required to form sulfilimine cross-links in collagen IV. J. Biol. Chem. 290 (35), 21741–21748.

Feng, X., Wang, Z., Fillmore, R., Xi, Y., 2014. MiR-200, a new star miRNA in human cancer. Cancer Lett. 344 (2), 166–173.

Gregory, P.A., Bert, A.G., Paterson, E.L., Barry, S.C., Tsykin, A., Farshid, G., Vadas, M.A., Khew-Goodall, Y., Goodall, G.J., 2008. The miR-200 family and miR-205 regulate epithelial to mesenchymal transition by targeting ZEB1 and SIP1. Nat. Cell Biol. 10 (5), 593–601.

Gudjonsson, T., Villadsen, R., Nielsen, H.L., Ronnov-Jessen, L., Bissell, M.J., Petersen, O.W., 2002. Isolation, immortalization, and characterization of a human breast epithelial cell line with stem cell properties. Genes Dev. 16 (6), 693–706.

Hanahan, D., Weinberg, R.A., 2011. Hallmarks of cancer: the next generation. Cell 144 (5), 646–674.

Hilmarsdottir, B., Briem, E., Bergthorsson, J.T., Magnusson, M.K., Gudjonsson, T., 2014. Functional role of the microRNA-200 family in breast morphogenesis and neoplasia. Genes 5 (3), 804–820.

Hilmarsdottir, B., Briem, E., Sigurdsson, V., Franzdottir, S.R., Ringner, M., Arason, A.J., Bergthorsson, J.T., Magnusson, M.K., Gudjonsson, T., 2015. MicroRNA-200c-141 and Np63 are required for breast epithelial differentiation and branching morphogenesis. Dev. Biol. 403 (2), 150–161.

Inoue, A., Seidel, M.G., Wu, W., Kamizono, S., Ferrando, A.A., Bronson, R.T., Iwasaki, H., Akashi, K., Morimoto, A., Hitzler, J.K., Pestina, T.I., Jackson, C.W., Tanaka, R., Chong, M.J., McKinnon, P.J., Inukai, T., Grosveld, G.C., Look, A.T., 2002. Slug, a highly conserved zinc finger transcriptional repressor, protects hematopoietic progenitor cells from radiation-induced apoptosis in vivo. Cancer Cell 2 (4), 279–288.

Javed, A., Lteif, A., 2013. Development of the human breast. Semin. Plast. Surg. 27 (1), 5–12.

Jayachandran, A., Prithviraj, P., Lo, P.H., Walkiewicz, M., Anaka, M., Woods, B.L., Tan, B., Behren, A., Cebon, J., McKeown, S.J., 2016. Identifying and targeting determinants of melanoma cellular invasion. Oncotarget 7 (27), 41186–41202.

Kal, A.J., van Zonneveld, A.J., Benes, V., van den Berg, M., Koerkamp, M.G., Albermann, K., Strack, N., Ruijter, J.M., Richter, A., Dujon, B., Ansorge, W., Tabak, H.F., 1999. Dynamics of gene expression revealed by comparison of serial analysis of gene expression transcript profiles from yeast grown on two different carbon sources. Mol. Biol. Cell 10 (6), 1859–1872.

Khan, K., Rudkin, A., Parry, D.A., Burdon, K.P., McKibbin, M., Logan, C.V., Abdelhamed, Z.I., Muecke, J.S., Fernandez-Fuentes, N., Laurie, K.J., Shires, M., Fogarty, R., Carr, I.M., Poulter, J.A., Morgan, J.E., Mohamed, M.D., Jafri, H., Raashid, Y., Meng, N., Piseth, H., Toomes, C., Casson, R.J., Taylor, G.R., Hammerton, M., Sheridan, E., Johnson, C.A., Inglehearn, C.F., Craig, J.E., Ali, M., 2011. Homozygous mutations in PXDN cause congenital cataract, corneal opacity, and developmental glaucoma. Am. J. Hum. Genet. 89 (3), 464–473.

Lawson, D.A., Werb, Z., Zong, Y., Goldstein, A.S., 2015. The cleared mammary fat pad transplantation assay for mammary epithelial organogenesis. Cold Spring Harb Protoc 2015 (12) (pdb.prot078071).

Lee, G.Y., Kenny, P.A., Lee, E.H., Bissell, M.J., 2007. Three-dimensional culture models of normal and malignant breast epithelial cells. Nat. Methods 4 (4), 359–365.

Lilja, A.M., Rodilla, V., Huyghe, M., Hannezo, E., Landragin, C., Renaud, O., Leroy, O., Rulands, S., Simons, B.D., Fre, S., 2018. Clonal analysis of Notch1-expressing cells reveals the existence of unipotent stem cells that retain long-term plasticity in the embryonic mammary gland. Nat. Cell Biol. 20 (6), 677–687.

Liu, Y., Carson-Walter, E.B., Cooper, A., Winans, B.N., Johnson, M.D., Walter, K.A., 2010. Vascular gene expression patterns are conserved in primary and metastatic brain tumors. J. Neuro-Oncol. 99 (1), 13–24.

Lloyd-Lewis, B., Davis, F.M., Harris, O.B., Hitchcock, J.R., Watson, C.J., 2018. Neutral lineage tracing of proliferative embryonic and adult mammary stem/progenitor cells. Development 145 (14).

Mani, S.A., Guo, W., Liao, M.J., Eaton, E.N., Ayyanan, A., Zhou, A.Y., Brooks, M., Reinhard, F., Zhang, C.C., Shipitsin, M., Campbell, L.L., Polyak, K., Brisken, C., Yang, J., Weinberg, R.A., 2008. The epithelial-mesenchymal transition generates cells with properties of stem cells. Cell 133 (4), 704–715.

Moes, M., Le Bechec, A., Crespo, I., Laurini, C., Halavatyi, A., Vetter, G., Del Sol, A., Friederich, E., 2012. A novel network integrating a miRNA-203/SNAI1 feedback loop which regulates epithelial to mesenchymal transition. PLoS One 7 (4), e35440.

Moustakas, A., Heldin, C.H., 2007. Signaling networks guiding epithelial-mesenchymal transitions during embryogenesis and cancer progression. Cancer Sci. 98 (10), 1512–1520.

Olson, P., Lu, J., Zhang, H., Shai, A., Chun, M.G., Wang, Y., Libutti, S.K., Nakakura, E.K., Golub, T.R., Hanahan, D., 2009. MicroRNA dynamics in the stages of tumorigenesis correlate with hallmark capabilities of cancer. Genes Dev. 23 (18), 2152–2165.

Pal, B., Chen, Y., Vaillant, F., Jamieson, P., Gordon, L., Rios, A.C., Wilcox, S., Fu, N., Liu, K.H., Jackling, F.C., Davis, M.J., Lindeman, G.J., Smyth, G.K., Visvader, J.E., 2017. Construction of developmental lineage relationships in the mouse mammary gland by single-cell RNA profiling. Nat. Commun. 8 (1), 1627.

Pechoux, C., Gudjonsson, T., Ronnov-Jessen, L., Bissell, M.J., Petersen, O.W., 1999. Human mammary luminal epithelial cells contain progenitors to myoepithelial cells. Dev. Biol. 206 (1), 88–99.

Peinado, H., Olmeda, D., Cano, A., 2007. Snail, ZEB and bHLH factors in tumour progression: an alliance against the epithelial phenotype? Nat. Rev. Cancer 7 (6), 415–428.

Peterfi, Z., Donko, A., Orient, A., Sum, A., Prokai, A., Molnar, B., Vereb, Z., Rajnavolgyi, E., Kovacs, K.J., Muller, V., Szabo, A.J., Geiszt, M., 2009. Peroxidasin is secreted and incorporated into the extracellular matrix of myofibroblasts and fibrotic kidney. Am. J. Pathol. 175 (2), 725–735.

Petersen, O.W., Polyak, K., 2010. Stem cells in the human breast. Cold Spring Harb. Perspect. Biol. 2 (5), a003160.

Petersen, O.W., Lind Nielsen, H., Gudjonsson, T., Villadsen, R., Ronnov-Jessen, L., Bissell, M.J., 2001. The plasticity of human breast carcinoma cells is more than epithelial to mesenchymal conversion. Breast Cancer Res. 3 (4), 213–217.

Pimentel, H., Bray, N.L., Puente, S., Melsted, P., Pachter, L., 2017. Differential analysis of RNA-seq incorporating quantification uncertainty. Nat. Methods 14 (7), 687–690.

Sarrio, D., Rodriguez-Pinilla, S.M., Hardisson, D., Cano, A., Moreno-Bueno, G., Palacios, J., 2008. Epithelial-mesenchymal transition in breast cancer relates to the basal-like phenotype. Cancer Res. 68 (4), 989–997.

Shimono, Y., Zabala, M., Cho, R.W., Lobo, N., Dalerba, P., Qian, D., Diehn, M., Liu, H., Panula, S.P., Chiao, E., Dirbas, F.M., Somlo, G., Pera, R.A., Lao, K., Clarke, M.F., 2009. Downregulation of miRNA-200c links breast cancer stem cells with normal stem cells. Cell 138 (3), 592–603.

Sigurdsson, V., Fridriksdottir, A.J., Kjartansson, J., Jonasson, J.G., Steinarsdottir, M., Petersen, O.W., Ogmundsdottir, H.M., Gudjonsson, T., 2006. Human breast microvascular endothelial cells retain phenotypic traits in long-term finite life span culture. In Vitro Cell. Dev. Biol. Anim. 42 (10), 332–340.

Sigurdsson, V., Hilmarsdottir, B., Sigmundsdottir, H., Fridriksdottir, A.J., Ringner, M., Villadsen, R., Borg, A., Agnarsson, B.A., Petersen, O.W., Magnusson, M.K., Gudjonsson, T., 2011. Endothelial induced EMT in breast epithelial cells with stem cell properties. PLoS One 6 (9), e23833.

Sitole, B.N., Mavri-Damelin, D., 2018. Peroxidasin is regulated by the epithelial-mesenchymal transition master transcription factor Snai1. Gene 646, 195–202.

Taube, J.H., Malouf, G.G., Lu, E., Sphyris, N., Vijay, V., Ramachandran, P.P., Ueno, K.R., Gaur, S., Nicoloso, M.S., Rossi, S., Herschkowitz, J.I., Rosen, J.M., Issa, J.P., Calin, G.A., Chang, J.T., Mani, S.A., 2013. Epigenetic silencing of microRNA-203 is required for EMT and cancer stem cell properties. Sci. Rep. 3, 2687.

Tauber, S., Jais, A., Jeitler, M., Haider, S., Husa, J., Lindroos, J., Knofler, M., Mayerhofer, M., Pehamberger, H., Wagner, O., Bilban, M., 2010. Transcriptome analysis of human

cancer reveals a functional role of heme oxygenase-1 in tumor cell adhesion. Mol. Cancer 9, 200.
Tindall, A.J., Pownall, M.E., Morris, I.D., Isaacs, H.V., 2005. Xenopus tropicalis peroxidasin gene is expressed within the developing neural tube and pronephric kidney. Dev. Dyn. 232 (2), 377–384.
Vidi, P.A., Bissell, M.J., Lelievre, S.A., 2013. Three-dimensional culture of human breast epithelial cells: the how and the why. Methods Mol. Biol. 945, 193–219.
Villadsen, R., Fridriksdottir, A.J., Ronnov-Jessen, L., Gudjonsson, T., Rank, F., LaBarge, M.A., Bissell, M.J., Petersen, O.W., 2007. Evidence for a stem cell hierarchy in the adult human breast. J. Cell Biol. 177 (1), 87–101.
Wellner, U., Schubert, J., Burk, U.C., Schmalhofer, O., Zhu, F., Sonntag, A., Waldvogel, B., Vannier, C., Darling, D., zur Hausen, A., Brunton, V.G., Morton, J., Sansom, O., Schuler, J., Stemmler, M.P., Herzberger, C., Hopt, U., Keck, T., Brabletz, S., Brabletz, T., 2009. The EMT-activator ZEB1 promotes tumorigenicity by repressing stemness-inhibiting microRNAs. Nat. Cell Biol. 11 (12), 1487–1495.
Wronski, A., Arendt, L.M., Kuperwasser, C., 2015. Humanization of the mouse mammary gland. Methods Mol. Biol. 1293, 173–186.
Wuidart, A., Sifrim, A., Fioramonti, M., Matsumura, S., Brisebarre, A., Brown, D., Centonze, A., Dannau, A., Dubois, C., Van Keymeulen, A., Voet, T., Blanpain, C., 2018. Early lineage segregation of multipotent embryonic mammary gland progenitors. Nat. Cell Biol. 20 (6), 666–676.
Yan, X., Sabrautzki, S., Horsch, M., Fuchs, H., Gailus-Durner, V., Beckers, J., Hrabe de Angelis, M., Graw, J., 2014. Peroxidasin is essential for eye development in the mouse. Hum. Mol. Genet. 23 (21), 5597–5614.
Young, C.D., Zimmerman, L.J., Hoshino, D., Formisano, L., Hanker, A.B., Gatza, M.L., Morrison, M.M., Moore, P.D., Whitwell, C.A., Dave, B., Stricker, T., Bhola, N.E., Silva, G.O., Patel, P., Brantley-Sieders, D.M., Levin, M., Horiates, M., Palma, N.A., Wang, K., Stephens, P.J., Perou, C.M., Weaver, A.M., O'Shaughnessy, J.A., Chang, J.C., Park, B.H., Liebler, D.C., Cook, R.S., Arteaga, C.L., 2015. Activating PIK3CA mutations induce an epidermal growth factor receptor (EGFR)/extracellular signal-regulated kinase (ERK) paracrine signaling Axis in basal-like breast Cancer. Mol. Cell. Proteomics 14 (7), 1959–1976.
Zhang, Z., Zhang, B., Li, W., Fu, L., Fu, L., Zhu, Z., Dong, J.T., 2011. Epigenetic silencing of miR-203 upregulates SNAI2 and contributes to the invasiveness of malignant breast Cancer cells. Genes Cancer 2 (8), 782–791.